

# Pressure-Induced Phase Transitions of Natural Brookite

Weixin Liu,<sup>†</sup> Jian Chen,<sup>†</sup> Xiaoliang Zhang,<sup>†</sup> Jinyuan Yan,<sup>‡</sup> Mingqiang Hou,<sup>†,‡</sup> Martin Kunz,<sup>‡</sup> Dongzhou Zhang,<sup>§</sup> and Hengzhong Zhang<sup>\*,†,ID</sup>

<sup>†</sup>Center for High Pressure Science and Technology Advanced Research, Shanghai 201203, China

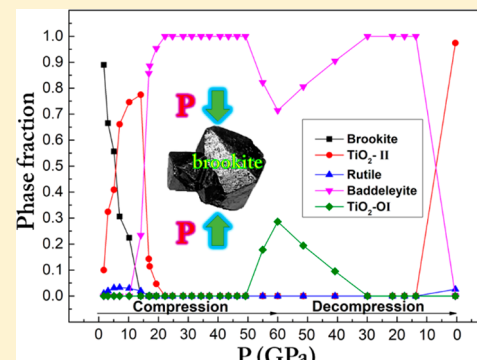
<sup>‡</sup>Advanced Light Source, Lawrence Berkeley National Laboratory, Berkeley, California 94720, United States

<sup>§</sup>Partnership for Extreme Crystallography Program, University of Hawaii at Manoa, Honolulu, Hawaii 96822, United States

## Supporting Information

**ABSTRACT:** The structures and stabilities of the high-pressure phases of titania ( $\text{TiO}_2$ ) are of great interest in the earth sciences, as these phases are the accessible analogs of component minerals in the earth's mantle. Brookite is a natural titania mineral, whose bulk phase is hard to synthesize in the laboratory, and its phase behavior at very high pressure remains unknown. Thus, in this work, using phase-pure natural brookite as the sample, we studied the phase transition of bulk brookite under compression up to ~60 GPa in three different pressure transmitting media. Results show that, at room temperature and in near hydrostatic conditions, brookite undergoes a series of transitions, i.e., brookite (~0–12 GPa)  $\rightarrow$   $\text{TiO}_2$ -II and minor rutile (~1–21 GPa)  $\rightarrow$  baddeleyite (~12–60 GPa)  $\rightarrow$   $\text{TiO}_2$ -OI (~33–60 GPa). Taking into account that all transitions occur at finite rates and that solidification of a pressure medium can influence transition kinetics, we show that the observed transition sequence is consistent with the expected high-pressure phase stability of  $\text{TiO}_2$  calculated from density functional theory. The knowledge obtained from this work may be used to infer the geological fate of brookite in nature.

**KEYWORDS:** titania, high pressure, phase transformation, nonhydrostaticity, pressure transmitting medium, shear modulus, equation-of-state, natural mineral



## INTRODUCTION

As a technologically important material, titania ( $\text{TiO}_2$ ) has applications in photocatalysis, gas sensors, energy storage, biotechnology, and cosmetics, etc. Natural titania exists mainly in the three polymorphs, rutile (tetragonal structure), anatase (tetragonal structure), and brookite (orthorhombic structure).<sup>1,2</sup> Studies show that, at ambient pressure, rutile is more stable than anatase at temperatures up to at least ~1000 °C.<sup>3</sup> Anatase and brookite are metastable with respect to rutile, and hence, they can transform to rutile upon heating above certain temperatures.<sup>4–7</sup> In nature, brookite often occurs in quartz veins of regional metamorphic rock series or as an accessory mineral in igneous rocks.<sup>8–10</sup> Brookite is relatively rare compared to rutile and anatase.<sup>11</sup> It is very difficult to synthesize bulk brookite in the laboratory, though nanocrystalline brookite can be prepared relatively easily in the laboratory using different methods.<sup>12–15</sup> Previous high-pressure (HP) studies on  $\text{TiO}_2$  predominantly focused on the phase transitions of bulk or nanocrystalline anatase and rutile. Titania phases involved in the subsequent high-pressure phase transitions include columbite ( $\text{TiO}_2$ -II, space group  $Pbcn$ ), baddeleyite (space group  $P2_1/c$ ),  $\text{TiO}_2$ -OI (space group  $Pbca$ ), and  $\text{TiO}_2$ -OII (space group  $Pnma$ ).<sup>16–19</sup> We only found scarce reports on high-pressure behaviors of nanocrystalline brookite at pressures up to ~28 GPa<sup>20</sup> and bulk brookite at

pressures up to ~10 GPa.<sup>11</sup> The phase behavior of bulk brookite at very high pressures ( $\gg 10$  GPa) remains unknown possibly because of the unavailability of bulk brookite from laboratory syntheses. However, such knowledge is needed to understand the detailed formation mechanism and stability of brookite. Thus, in this work, using phase-pure natural brookite as the starting material, we studied the pressure-induced phase transitions of natural brookite at room temperature and at pressures up to ~60 GPa using *in situ* high-pressure X-ray diffraction (XRD) and Raman spectroscopy. We aim to obtain knowledge about the phase behavior and structural stability of bulk brookite under compression to very high pressures (and in subsequent decompression as well) so that insights into the history and possible fate of natural brookite minerals can be generated with new experimental data.

## EXPERIMENTAL SECTION

**Sample.** The natural brookite sample used in this study was from the mineral collection no. 8115 of the Department of Earth and Planetary Science, University of California Berkeley.

Received: December 24, 2018

Revised: April 1, 2019

Accepted: April 8, 2019

Published: April 9, 2019

The mineral was sourced from Magnet Cove, AR, USA. It is similar in appearance to those described in refs 8 and 9. A few brookite crystals with well-developed morphologies were chosen. The crystals were immersed in a nitric acid solution ( $1 \text{ mol L}^{-1}$ ) to dissolve their surface stains and then washed with deionized water before drying and crushing into small pellets. Then, the pellets were ground with a mortar and pestle to very fine powders that were used for the high-pressure study in this work (below).

**X-ray Powder Diffraction.** To examine the crystal structures of the natural  $\text{TiO}_2$  sample, XRD patterns were obtained using an X-ray powder diffractometer (Malvern Panalytical) with  $\text{Cu K}\alpha$  radiation (wavelength,  $1.54056 \text{ \AA}$ ). The XRD patterns were collected from  $2\theta = 10$  to  $80^\circ$  at a scanning rate of  $5^\circ/\text{min}$ .

**Scanning Electron Microscopy and Energy Dispersive Spectroscopy.** The morphologies, particle sizes, and elemental compositions of the ground titania particles were examined using a scanning electron microscope (SEM; VERSA 3D, FEI) equipped with an energy dispersive spectrometer (EDS), which were operated under  $5.0 \text{ kV}/27 \text{ pA}$  and  $15.0 \text{ kV}/0.21 \text{ nA}$ , respectively.

**In Situ High-Pressure XRD and Raman Spectroscopy.** A diamond anvil cell (DAC) was used to generate the required high pressure of the sample. The culet size of the anvils was  $300 \mu\text{m}$  in diameter. A stainless steel gasket was preindented to  $23 \mu\text{m}$  in thickness, and then a hole of  $150 \mu\text{m}$  in diameter was drilled through the center of the indentation using laser drilling (at HPSTAR), serving as the sample chamber. A tiny amount of the finely ground brookite powder was compressed into a thin foil at a pressure of  $\sim 8 \text{ MPa}$  using a powder pressing machine. Then, one piece of the thin foil  $\sim 15 \mu\text{m}$  thick and an appropriate size for the sample chamber were chosen for loading into the DAC together with a few grains of ruby as the pressure calibrant. A pressure transmitting medium was loaded into the DAC afterward. Helium, neon, and methanol–ethanol mixture (4:1 in volume) were used as the pressure transmitting media for the HP-XRD measurements; a methanol–ethanol mixture (4:1 in volume) was used as the pressure transmitting medium for the HP–Raman spectroscopy measurements.

In situ HP-XRD measurements were performed at the 12.2.2 beamline station of the Advanced Light Source (ALS) at room temperature.<sup>21,22</sup> HP-XRD patterns were collected at an X-ray wavelength of  $0.4959 \text{ \AA}$  using a MAR345 image plate detector. The sample-to-detector distance was calibrated using a  $\text{CeO}_2$  standard. After compressing the sample near the required pressure value and equilibrating the system for  $\sim 10 \text{ min}$ , the sample pressure was measured using laser fluorescence (excitation laser wavelength,  $447 \text{ nm}$ ). Then, the HP-XRD measurement at the given pressure was conducted in the beamline station, taking  $\sim 5 \text{ min}$  to complete. The HP-XRD and the pressure measurements were repeated at all pressures in the full compression–decompression cycle.

Additional HP-XRD data were collected at the 13-BM-C beamline station of the Advanced Photon Source (APS) at room temperature with an X-ray wavelength of  $0.4340 \text{ \AA}$ . At 13-BM-C, a MAR165 CCD detector was used to collect the diffraction image and a NIST standard  $\text{LaB}_6$  sample was used to calibrate the sample-to-detector distance and the detector tilt. The pressure measurements were similar to those at ALS-12.2.2 (above) except that the excitation laser had a wavelength of  $532 \text{ nm}$ . The sample pressure was measured

after equilibrating the system for  $\sim 6 \text{ min}$ , and the HP-XRD measurement at each given pressure took  $\sim 2 \text{ min}$  to complete.

The diffraction images were integrated using the Dioptas program<sup>23</sup> to yield numerical intensity vs  $2\theta$  data. Rietveld-fitting analyses were performed on the collected XRD patterns using GSAS software<sup>24,25</sup> to identify and/or verify the phases present and to obtain the phase contents of the titania phases as a function of pressure.

High-pressure Raman data were collected from 100 to  $800 \text{ cm}^{-1}$  at room temperature using a Raman spectrometer (inVia Reflex, Renishaw) with a  $532 \text{ nm}$  excitation laser at  $\sim 10\%$  of the laser power ( $83.3 \text{ mW}$ ). The integration time was  $0.029 \text{ s}$  for each incremental step of  $1 \text{ cm}^{-1}$ . At a given pressure, the collection of one Raman spectrum took  $\sim 20 \text{ s}$ .

## ■ COMPUTATIONAL SECTION

The enthalpies of the concerned  $\text{TiO}_2$  phases (brookite, anatase, rutile, baddeleyite,  $\text{TiO}_2$ -II, and  $\text{TiO}_2$ -OI) at different pressures were calculated using density functional theory (DFT) implemented in the Quantum Espresso (QE) package.<sup>26</sup> The computations were conducted using an integrated graphic user interface and a running environment of QE, Burai (v.1.3.2).<sup>27</sup> The projector augmented-wave (PAW) pseudopotential functions<sup>28</sup> of Ti and O with an energy cutoff of  $\sim 52 \text{ Ry}$  and charge density cutoff of  $\sim 575 \text{ Ry}$ , and PBE exchange–correlations<sup>29</sup> at the GGA+U approximation<sup>30</sup> were used for the calculations, where the Hubbard correction parameter U was taken as  $5.0 \text{ eV}$  for both the Ti and O atoms.<sup>31</sup> At a given pressure, the crystal structure of a Ti–O phase was optimized and the enthalpy of the phase was obtained. The enthalpy relative to rutile at the same pressure could then be calculated and used to determine the relative phase stability of various titania phases at different pressures.

The enthalpy of a high-pressure titania phase (baddeleyite or  $\text{TiO}_2$ -OI) was also calculated under compression with unequal pressures acting on different crystallographic orientations of the crystal (see Figure S1 and Table S1, *Supporting Information (SI)*). First, the crystal was hydrostatically compressed in all orientations at a pressure  $P$ , generating a geometrically optimized structure and enthalpy. Then, the crystal was non-hydrostatically compressed under an axial pressure of  $P_{\text{ax}}/\text{GPa} = P + 5$  and two perpendicular radial pressures of  $P_{\text{rad}} = P$  under the constraint that only the axial dimension was free to change. This produced another geometrically optimized structure and enthalpy. The enthalpy of the non-hydrostatic case (at  $P_{\text{ax}}/\text{GPa} = P + 5$  and  $P_{\text{rad}} = P$ ) relative to that of the hydrostatic case (at  $P_{\text{ax}}/\text{GPa} = P + 5$ ) reflects the effect of the non-hydrostaticity on the enthalpy of the high-pressure phase.

## ■ RESULTS AND DISCUSSION

**Sample Characterization.** A photograph of the natural brookite crystals is shown in Figure 1a. The single crystals are black in color and have pseudohexagonal bipyramidal shapes with sizes ranging from  $\sim 2.2$  to  $4.5 \text{ mm}$ . One of the crystals is twinned with another smaller one.

The XRD pattern at ambient pressure of the brookite sample is shown in Figure 1b. Rietveld analysis confirmed that the sample is a single-phase brookite (ICSD No. 15409<sup>32</sup>), since all of the diffraction peaks can be indexed as reflections from the brookite structure in the  $Pbca$  space group.<sup>33</sup> The XRD pattern of the brookite thin foil for loading into the DAC is



**Figure 1.** (a) Photograph of natural brookite crystals; (b) Rietveld fitting of the X-ray diffraction pattern of natural brookite at ambient pressure.

almost identical to that of the powder sample before pressing (Figure S2). This indicates that no phase transition had occurred in the preprocessing of the brookite sample before applying GPa-scale pressures in the DAC.

Figure 2a shows the SEM image of the ground fine brookite particles. Two locations of a particle were chosen for elemental analysis using EDS (Figure 2b); the corresponding EDS spectra are shown in Figure 2c,d. EDS results (Table 1) show that the natural brookite sample consists of  $\text{TiO}_2$  (atomic ratio of  $\text{Ti}:\text{O} \approx 1:2$ ) with trace amount of niobium that causes the black color of the natural brookite crystals.<sup>8,10</sup>

**In Situ High-Pressure XRD.** Figure 3 shows the HP-XRD patterns of natural brookite under compression using three different kinds of pressure ( $P$ ) transmitting media: helium (Figure 3a), neon (Figure 3b,c), and a methanol–ethanol mixture (Figure 3d,e) at pressures up to  $\sim 60$  GPa. According to ref 34, He, Ne, and the methanol–ethanol mixture solidify at 12.1, 4.8, and 10.5 GPa at room temperature, respectively. Before their solidification, they are all hydrostatic; i.e., the deviatoric stress across a sample is  $\sim 0$  GPa. Even after solidification, in a gasket bore of  $80\text{--}200\ \mu\text{m}$ , the deviatoric stress is  $<0.15$  at 40 GPa in He and  $<0.5$  at 50 GPa in Ne,<sup>34</sup> which make them quasi-hydrostatic in a wide range of pressures. However, in the methanol–ethanol mixture, the deviatoric stress increases dramatically with pressure; e.g., it is  $\sim 2.5$  GPa at  $\sim 22$  GPa.<sup>34</sup> Thus, the non-hydrostaticity of the three pressure media increases in the order of helium, neon, and methanol–ethanol mixture. Using the three  $P$  media

allows us to investigate the influences of their hydrostaticity and elastic properties on the phase transition of natural bulk brookite.

The XRD patterns of the bulk brookite under compression in helium are shown in Figure 3a. A series of phase transitions occurred during compression of the sample. By comparing these with the calculated XRD patterns of reference  $\text{TiO}_2$  phases (bottom of Figure 3a) and using Rietveld analyses (representative fittings are shown in Figure 4), the present phases were identified. Rietveld analyses show that small amounts of  $\text{TiO}_2$ -II phase (space group,  $Pbcn$ ; ICSD No. 15328<sup>32</sup>) and rutile (space group,  $P4_2/mnm$ , ICSD No. 9161<sup>32</sup>) appeared at pressures as low as 0.8 GPa (Figure 4a). At 9.4 GPa, the majority of brookite had transformed to  $\text{TiO}_2$ -II and minor rutile. At 14.3 GPa, brookite disappeared. Meanwhile, the formed  $\text{TiO}_2$ -II and the minor rutile started to transform to baddeleyite (space group,  $P2_1/c$ ; COD No. 9015355<sup>35</sup>), and the transformations completed at  $\sim 23.7$  GPa (Figure 3a). The baddeleyite phase remained a single phase between 23.7 and 29.7 GPa, above which it started to transform to and coexist with  $\text{TiO}_2$ -OI (space group,  $Pbca$ <sup>18</sup>) up to the maximum experimental pressure (59.7 GPa) (Figure 3a). The coexistence of the two phases in such a wide pressure range ( $\sim 35\text{--}60$  GPa; Figure 3a) may be attributed to the similarity between the two structures.<sup>36–39</sup> During decompression,  $\text{TiO}_2$ -OI converted back to baddeleyite (Figure 3a). When decompressed to 13.6 GPa,  $\text{TiO}_2$ -OI disappeared, while  $\text{TiO}_2$ -II and small amounts of rutile reappeared, coexisting with baddeleyite. Upon full decompression to  $\sim 0.1$  GPa, baddeleyite converted almost fully to  $\text{TiO}_2$ -II coexisting with a small amount of rutile (Figure 3a). From the Rietveld analyses of all the XRD patterns in Figure 3a, the variations of the phase contents of various titania phases with pressure are depicted in Figure 5a. This diagram shows clearly the phase behavior of bulk brookite under compression in a helium medium.

Similarly, the phases present during compression and decompression in the neon pressure medium (Figure 3b,c) or methanol–ethanol mixture (Figure 3d,e) were identified using the same methods as the one used for Figure 3a. The variations of the phase contents with pressure in these two media are illustrated in Figure 5b,c, respectively. The three diagrams in Figure 5 show that the phase behaviors of bulk brookite in both helium and neon are similar at all  $P$ , indicating that their (quasi-) hydrostaticities are nearly equal and affect the phase behavior of brookite in the same way. Phase transitions of bulk brookite in the methanol–ethanol mixture (Figure 5c) are also similar to those in helium (Figure 5a) and neon (Figure 5b) in the hydrostatic pressure range ( $<11$  GPa<sup>34</sup>). However, they deviate from those in the latter two media significantly at  $>\sim 11$  GPa: in methanol–ethanol, the baddeleyite phase fully formed from brookite at  $\sim 25$  GPa could remain up to  $\sim 50$  GPa before transforming to  $\text{TiO}_2$ -OI (Figure 5c), while, in helium and neon, the baddeleyite also fully formed at  $\sim 25$  GPa but started to transform to  $\text{TiO}_2$ -OI as low as  $\sim 30$  GPa (Figure 5a,b). Moreover, during decompression, baddeleyite could also retain its single phase between  $\sim 30$  and  $\sim 15$  GPa in the methanol–ethanol medium (Figure 5c), while, in helium and neon, no single baddeleyite phase was observed (Figure 5a,b). These differences demonstrate that the hydrostaticity and the related elasticity of a pressure medium can modify the phase behavior of titania markedly: non-hydrostaticity favors stabilization of the

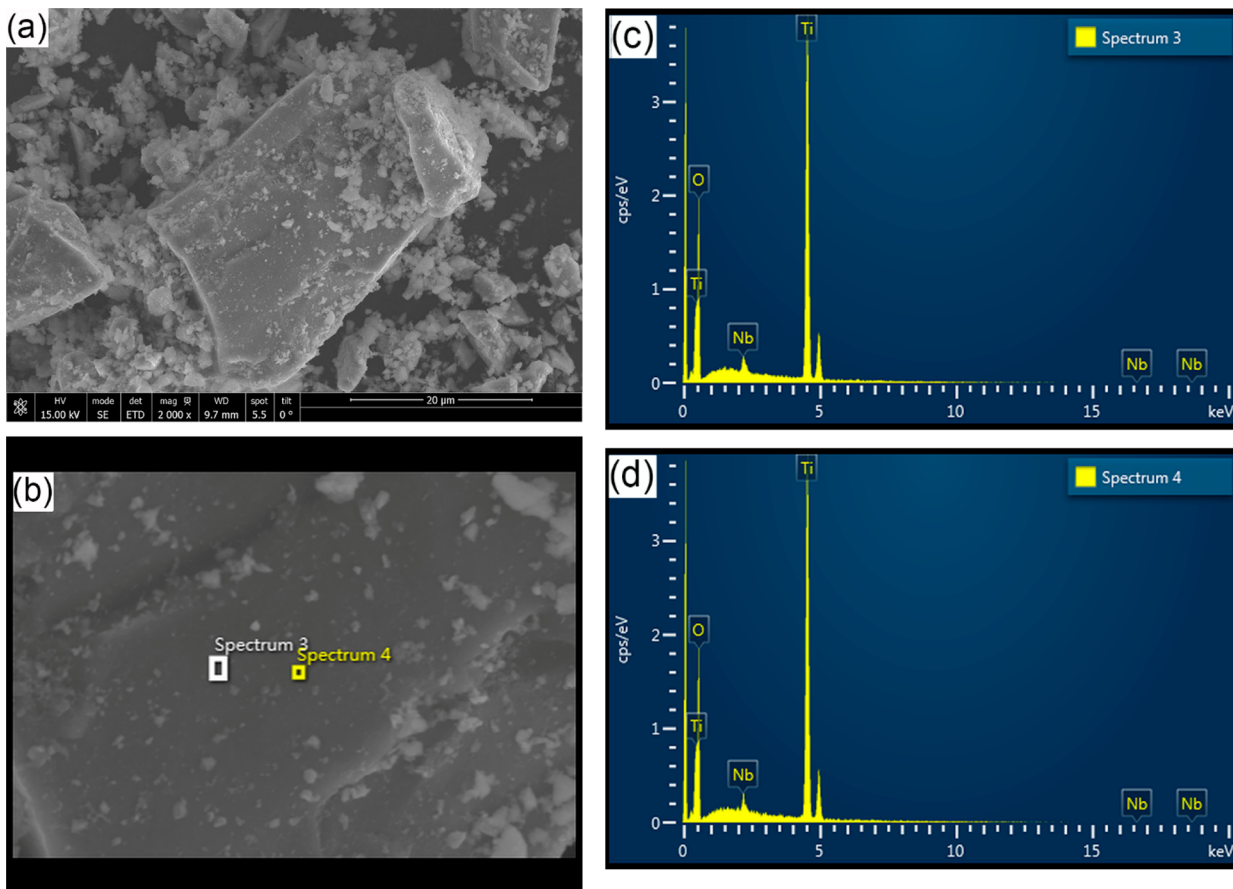


**Figure 2.** SEM image of the natural brookite particles produced from crushing and grinding a brookite crystal (a); chosen sample locations for the EDS analyses (b); EDS spectra from the chosen locations (c, d).

**Table 1. Major Chemical Composition of the Natural Brookite Sample**

element	av wt percent (%)	av at. percent (%)
O	38.64	65.72
Ti	59.23	33.65
Nb	2.13	0.63
total	100	100

baddeleyite phase as a single phase. This phenomenon may be interpreted as a result of the solidification of the methanol–ethanol mixture, as the solidified glassy and stiff mixture can introduce lattice strains in the titania phases, impacting the transition kinetics. Because baddeleyite has a lower symmetry (monoclinic) than the other occurring phases (either orthorhombic or tetragonal), it can accommodate more lattice strains (due to less geometric constraint on the unit cell) than them (due to more geometric constraints on the unit cells). Thus, non-hydrostaticity (and related medium properties) tends to slow or even inhibit the transition from baddeleyite to  $\text{TiO}_2\text{-OI}$ .

Figure 5 should be treated as non-equilibrium (i.e., kinetic) state diagrams as they deal with the behavior of a metastable phase (brookite), show the path-dependent behavior (e.g., difference between compression and decompression), and do not conform to the equilibrium phase rule. If the  $\text{TiO}_2$  system were to be in equilibrium at room temperature under compression, the maximum number of coexisting phases is  $P = C + 1 - F = 1 + 1 - 0 = 2$ . However, in our experiments, three phases occurred concurrently at some pressures (e.g., at 9.4 GPa in compression in Figure 5a). This happened because non-hydrostatic stress provides an additional degree of freedom at some of the experimental conditions, allowing the occurrence of competing phase transitions from one phase (or two phases) to the other two phases (or another phase). For instance, at 9.4 GPa in compression, brookite  $\rightarrow \text{TiO}_2\text{-II}$  and brookite  $\rightarrow$  rutile (Figures 3a and 5a).

$= C + 1 - F = 1 + 1 - 0 = 2$ . However, in our experiments, three phases occurred concurrently at some pressures (e.g., at 9.4 GPa in compression in Figure 5a). This happened because non-hydrostatic stress provides an additional degree of freedom at some of the experimental conditions, allowing the occurrence of competing phase transitions from one phase (or two phases) to the other two phases (or another phase). For instance, at 9.4 GPa in compression, brookite  $\rightarrow \text{TiO}_2\text{-II}$  and brookite  $\rightarrow$  rutile (Figures 3a and 5a).

**High-Pressure Raman Spectroscopy.** High-pressure Raman measurements of the natural bulk brookite (Figure 6) were conducted to confirm the phase transitions observed by XRD (Figure 3d,e). As shown in Figure 6a, the Raman peaks observed at 1.1 GPa are in good agreement with the predicted vibrational bands of brookite:<sup>40</sup>  $A_{1g}$  (127, 155, 192, 246, 414, and  $643\text{ cm}^{-1}$ ),  $B_{1g}$  (136, 155, 213, 322, 414, and  $504\text{ cm}^{-1}$ ),  $B_{2g}$  (366, 464, and  $586\text{ cm}^{-1}$ ), and  $B_{3g}$  (172, 286, 547, and  $449\text{ cm}^{-1}$ ),<sup>40,41</sup> among which the band at  $155\text{ cm}^{-1}$  is the strongest. Upon further compression to 5.8 GPa, the Raman bands of the  $\text{TiO}_2\text{-II}$  phase<sup>42–44</sup> became obvious, while the Raman bands of brookite became weak and almost disappeared at 11.1 GPa. When the pressure reached 19.8 GPa, all  $\text{TiO}_2\text{-II}$  Raman peaks disappeared, while the baddeleyite Raman peaks<sup>42–44</sup> appeared and then became significantly broader and weaker under further compression to 45.0 GPa. From 49.3 to 59.6 GPa, a sharp Raman peak at  $\sim 295\text{ cm}^{-1}$  appeared, indicating the  $\text{TiO}_2\text{-OI}$  phase, and hence, the Raman spectra consisted of contributions from both the baddeleyite and  $\text{TiO}_2\text{-OI}$  phases.

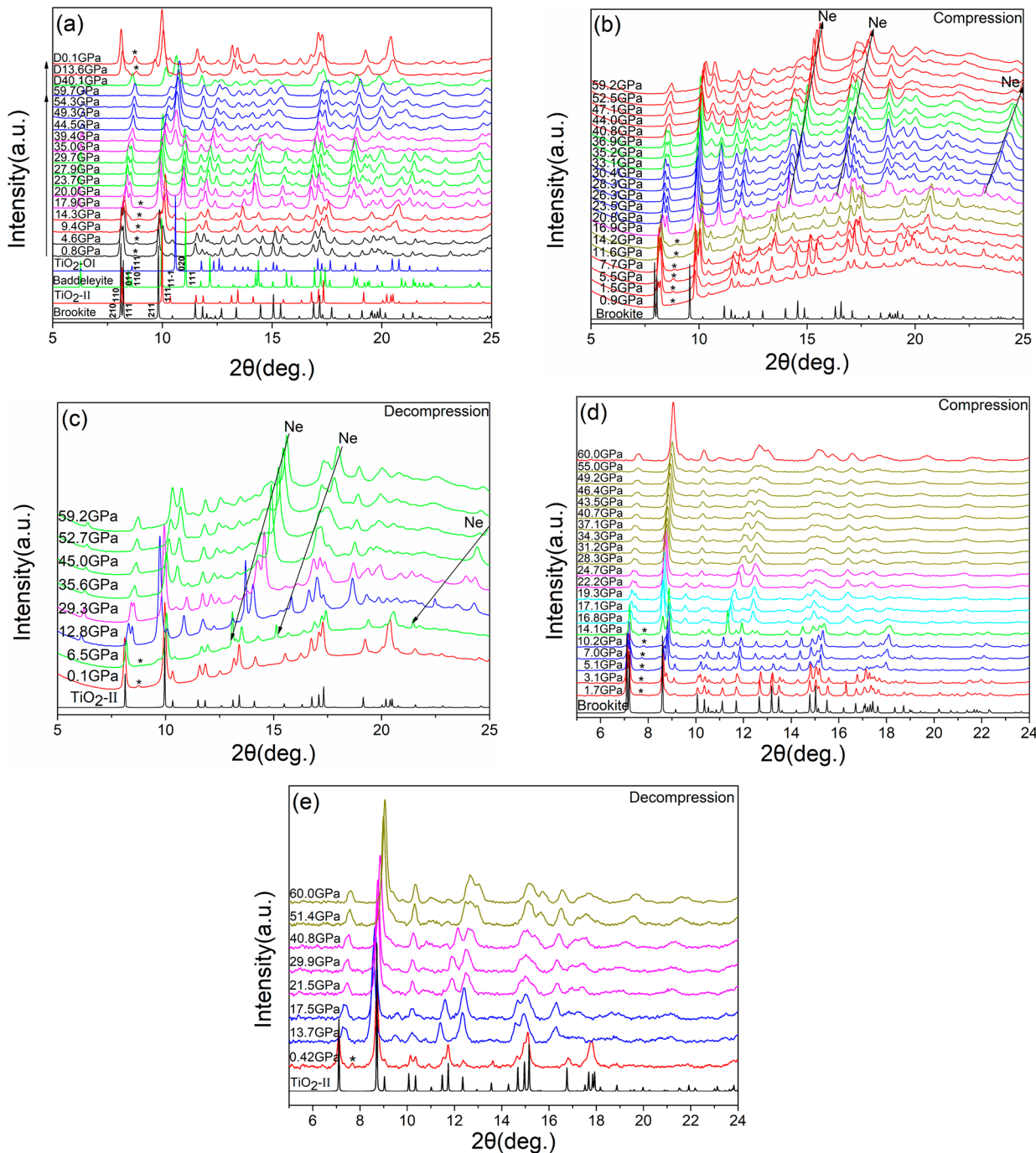


**Figure 3.** High-pressure XRD patterns of natural brookite under compression using pressure transmitting media of helium (a), neon (b and c), and methanol–ethanol (4:1 in volume; d, e). Data in panels a–c were collected at ALS-12.2.2 beamline station, and those in panels d and e at the APS-13-BMC beamline station. In panel a, prefix “D” in the pressure values indicates decompression. The calculated XRD patterns under ambient pressure are shown at the very bottom of each diagram for reference. Asterisk symbols (\*) denote rutile (110) peaks.

During decompression from 59.6 to 33.0 GPa (Figure 6b), the TiO<sub>2</sub>-OI Raman peaks became progressively weaker while those of baddeleyite became stronger. On further decompression to 13.2 GPa, the Raman spectra were dominated by baddeleyite. When the pressure decreased to 2.9 GPa, the TiO<sub>2</sub>-II Raman bands increased significantly, which were retained at 1.0 GPa. Rutile Raman bands were not observed in decompression to near the ambient pressure, as would be expected from the XRD data (Figure 5c). We interpret this as being due to the very low content of rutile. Overall, the high-pressure Raman spectroscopy data of the phase transitions of

natural brookite in a methanol–ethanol *P* medium are in good agreement with the XRD results (Figure 5c).

In the Raman measurements, laser illumination on a sample might produce heat, causing thermally activated phase transitions in brookite. However, as the applied laser power was low and the exposure time was short (see above), any heat generated could be easily dissipated into the gasket via the pressure medium and then to the DAC set. In addition, the thermally activated brookite-to-rutile transition requires very high temperature (over 800 °C).<sup>45</sup> This temperature is unlikely to have been achieved by the Raman laser illumination in our

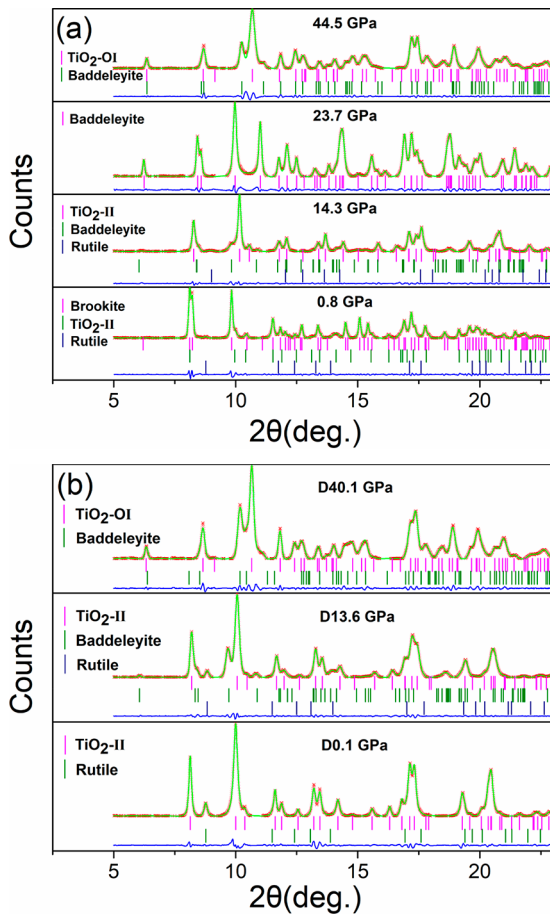


**Figure 4.** Representative Rietveld fitting of XRD patterns (shown in Figure 3a) of natural brookite during compression (a) and decompression (b). The derived lattice parameters and phase contents are listed in Table S2.

experiments. Thus, the phase transitions observed in the HP-Raman measurements can all be attributed to the pressure effects.

**Sequences of Phase Transitions of Bulk Brookite under Compression.** Our experimental results (Figure 5) show that, under compression, bulk brookite follows the phase transition sequence of brookite  $\rightarrow$   $\text{TiO}_2\text{-II}$  (+minor rutile)  $\rightarrow$  baddeleyite  $\rightarrow$   $\text{TiO}_2\text{-OI}$ , whereas during decompression it is  $\text{TiO}_2\text{-OI} \rightarrow$  baddeleyite  $\rightarrow$   $\text{TiO}_2\text{-II}$  (+minor rutile). In comparison, nanobrookite transforms to baddeleyite directly.<sup>20</sup> Such a difference may be related to the increased free energy of nanoparticles, which is size- and morphology-dependent, causing modified phase behavior and transition sequence in nanoparticles.<sup>46</sup>

Previous experimental and theoretical works show that, under compression, bulk anatase or rutile follows the phase transition sequence of anatase/rutile  $\rightarrow$   $\text{TiO}_2\text{-II} \rightarrow$  baddeleyite  $\rightarrow$   $\text{TiO}_2\text{-OI} \rightarrow$   $\text{TiO}_2\text{-OII}$ .<sup>18,19,47–49</sup> In this respect, the pressure-induced phase transitions of bulk brookite resemble those of bulk anatase and bulk rutile. However, the observed temperatures for the  $\text{TiO}_2\text{-OI}$  phase formation are quite different, as discussed below.

Theoretical calculations predicted the presence of  $\text{TiO}_2\text{-OI}$  in the pressure range of  $\sim 45\text{--}70$  GPa (300 K),<sup>18</sup> above  $\sim 40$  GPa (0 K),<sup>18</sup> or in  $\sim 20\text{--}40$  GPa (0 K).<sup>50</sup> Experimentally,  $\text{TiO}_2\text{-OI}$  occurred at 1300–1500 K by laser heating and in the

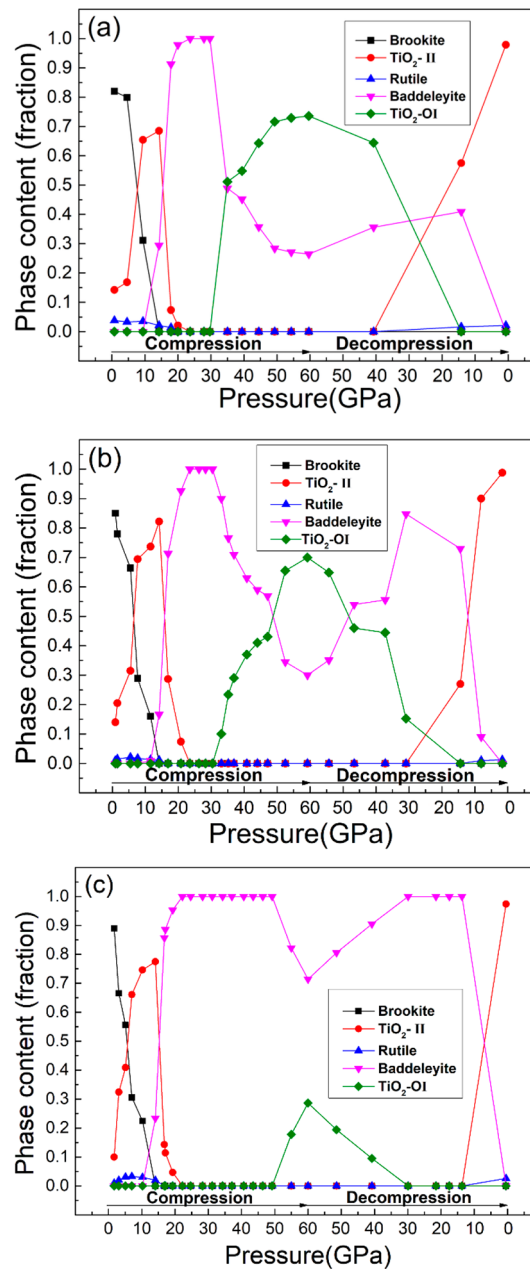


**Figure 5.** Pressure dependence of phase contents of  $\text{TiO}_2$  phases occurring during the compression and decompression of the natural brookite sample using pressure transmitting media of helium (a), neon (b), and methanol–ethanol (4:1 in volume; c).

pressure range of 28–32 GPa.<sup>18</sup> In another experiment,  $\text{TiO}_2\text{-OI}$  was observed at 2200–2500 K in laser heating and in the pressure range of 35.3–36.2 GPa.<sup>51</sup> In contrast to these,  $\text{TiO}_2\text{-OI}$  formed at room temperature at  $\sim 33$  GPa in helium/neon media (Figure 5a,b) or  $\sim 50$  GPa in methanol–ethanol medium (Figure 5c) in our experiments using bulk brookite as the starting material. Moreover, the formed  $\text{TiO}_2\text{-OI}$  was stable at  $P$  up to the maximum experimental pressure of  $\sim 60$  GPa. The formation pressure of bulk  $\text{TiO}_2\text{-OI}$  in quasi-hydrostatic conditions ( $\sim 33$  GPa) is far less than the predicted pressure of 45–70 GPa.<sup>18</sup> Yet, it is close to the experimentally observed pressures in the laser heating experiments of  $\sim 28\text{--}32$  GPa<sup>18</sup> or  $\sim 35\text{--}36$  GPa.<sup>51</sup> These indicate that using brookite as

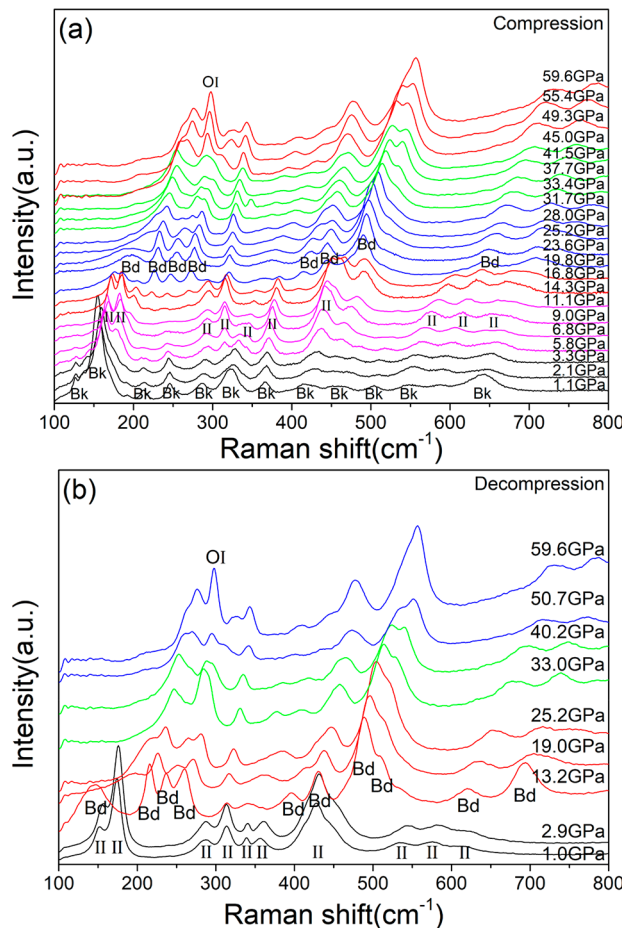


**Figure 6.** High-pressure Raman spectra of natural brookite under compression (a) and decompression (b) using a methanol–ethanol mixture (4:1 in volume) as the pressure transmitting medium. “Bk”, “Bd”, “OI”, and “II” denote brookite, baddeleyite, TiO<sub>2</sub>-OI, and TiO<sub>2</sub>-II ( $\alpha$ -PbO<sub>2</sub>) phases, respectively.

the starting material can alter the phase transition kinetic route so that the kinetic barrier can be reduced significantly.

Figure 5 reveals that, in the methanol–ethanol medium at high pressure, the non-hydrostaticity and the change in the medium elasticity (see below) can inhibit the baddeleyite  $\rightarrow$  TiO<sub>2</sub>-OI transition (Figure 5c vs Figure 5a,b), making the transition pressure ( $\sim$ 50 GPa) much higher than those in more hydrostatic conditions ( $\sim$ 33 GPa). In previous laser heating experiments, no pressure medium<sup>18</sup> or NaCl medium<sup>51</sup> was used, which would produce less or no hydrostatic conditions. Again, this would introduce high lattice strain in baddeleyite, stabilizing baddeleyite at high pressures (see above). Consequently, much higher temperatures ( $>1000$  °C) were needed to trigger the baddeleyite  $\rightarrow$  TiO<sub>2</sub>-OI transition with laser heating in these works.<sup>18,51</sup>

**Understanding the Phase Transition Sequences of Brookite Using Computations.** The phase stabilities at both ambient and high pressures of various titania phases have been studied extensively using different kinds of computational methods,<sup>31,50,52–56</sup> achieving different levels of success in terms of consistency with the available experimental data. It was proven that it is nontrivial to correctly model the phase stability of the titania system as a function of either or both of the temperatures and pressures.<sup>31</sup> For example, to correctly reproduce the observed high-pressure phase transitions among

anatase, rutile, and TiO<sub>2</sub>-II using the DFT+U method, the Hubbard parameter  $U$  should equal 5 eV.<sup>31</sup> Based on this, we chose  $U = 5$  eV in our computations using the DFT+U method. Figure 7 shows our calculated enthalpies of the

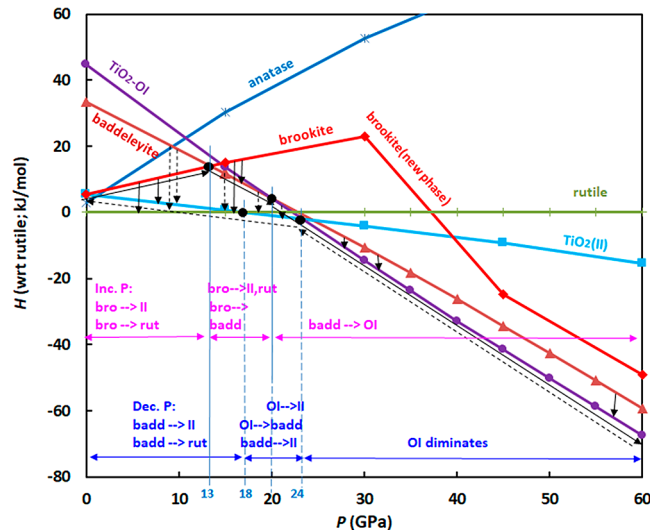


**Figure 7.** Calculated enthalpies of titania phases relative to that of rutile as a function of pressure. The downward solid (dashed) arrow indicates a possible phase transition from a high-enthalpy phase to a low-enthalpy phase during compression (decompression); the slanted solid and dashed arrows denote the enthalpy routes in compression and decompression, respectively; the solid (dashed) vertical line indicates the energy crossover between the two phases during compression (decompression). The drastic slope change of the enthalpy curve of brookite at 30 GPa is due to its spontaneous change to a new structure (phase) in the DFT geometric optimization.

concerned titania phases at different pressures. Using the calculated lattice parameters and, hence, the unit cell volumes as a function of pressure, we also derived the bulk moduli of several TiO<sub>2</sub> phases by fitting the data to the equations-of-state (EOS) (see Figure S3). Results in Table S3 show that the DFT-derived bulk moduli agree fairly well with those derived from the experimental data (Figure S4). By contrast, the bulk moduli from a previous DFT work<sup>57</sup> without the Hubbard correction deviate appreciably from the experimental results (except for TiO<sub>2</sub>-II).

Our DFT calculation results show that, at ambient temperature and pressure,  $\Delta H(\text{rutile} \rightarrow \text{anatase}) = 3.0$  kJ mol<sup>-1</sup> and  $\Delta H(\text{rutile} \rightarrow \text{brookite}) = 5.5$  kJ mol<sup>-1</sup> (Figure 7). Using the experimentally determined entropies of rutile (50.4 J mol<sup>-1</sup> K<sup>-1</sup>),<sup>3</sup> anatase (49.8 J mol<sup>-1</sup> K<sup>-1</sup>),<sup>3</sup> and brookite (52.6 J mol<sup>-1</sup> K<sup>-1</sup>),<sup>58</sup> the entropy contribution to the free energy change is  $-T\Delta S(\text{rutile} \rightarrow \text{anatase}) = 0.2$  kJ mol<sup>-1</sup> and  $-T\Delta S(\text{rutile} \rightarrow \text{brookite}) = -0.7$  kJ mol<sup>-1</sup>, accounting for 6.2% and 14.6% of the total free energy change (i.e.,  $|T\Delta S / (\Delta H - T\Delta S)|$ ), respectively. As the pressure increases, the entropy contribution ( $|T\Delta S / (\Delta U + P\Delta V - T\Delta S)|$ ) decreases. Based on this, and considering that experimental entropies of other involving phases are unavailable, we used the enthalpies of the TiO<sub>2</sub> phases to analyze the phase transitions of TiO<sub>2</sub>.

Figure 7 shows possible phase transitions following the enthalpy routes during brookite compression and decompression, taking into account the transition kinetics (i.e., a transition only proceeds at a limited rate rather than instantaneously). During compression at  $P$  below 13 GPa,

brookite is metastable with respect to rutile and  $\text{TiO}_2\text{-II}$ . Thus, brookite can transform to rutile and  $\text{TiO}_2\text{-II}$  via competing reactions. This is consistent with the experimental data (Figures 3 and & 5) that show the formation of  $\text{TiO}_2\text{-II}$  and rutile from brookite. The experimentally formed rutile has a lower content than  $\text{TiO}_2\text{-II}$ , while in Figure 7 at  $P < 18 \text{ GPa}$ , rutile has a lower enthalpy and, hence, it should be more stable and have a higher content than  $\text{TiO}_2\text{-II}$ . If the entropies of the involved phases<sup>52,58</sup> are considered,  $\Delta G(\text{brookite} \rightarrow \text{rutile}) = -5.5 - 0.3 \times (51.4 - 52.6) = -5.1 \text{ kJ mol}^{-1}$  and  $\Delta G(\text{brookite} \rightarrow \text{TiO}_2\text{-II}) = (5.4 - 5.5) - 0.3 \times (48.4 - 52.6) = 1.16 \text{ kJ mol}^{-1}$  at ambient pressure. This means that, around ambient pressure, the transition from brookite to rutile is even more thermodynamically favorable than brookite to  $\text{TiO}_2\text{-II}$ . Thus, the difference between the theoretical expectation and the experimental data suggests that there is a faster transition kinetics from brookite to  $\text{TiO}_2\text{-II}$  than to rutile due to the similarity between the  $\text{TiO}_2\text{-II}$  and brookite structures, as they differ only in the stacking arrangement of similar structural layers.<sup>4,59</sup> On compression between 13 and 20 GPa, unreacted brookite continues to transform to  $\text{TiO}_2\text{-II}$  and rutile, and to baddeleyite, as the enthalpy of the latter now becomes lower than that of brookite (Figure 7). This also agrees with the experimental data in Figure 5, though experimentally the contents of rutile and  $\text{TiO}_2\text{-II}$  diminish with the increase of  $P$ . The fast increase of the baddeleyite content above  $\sim 15 \text{ GPa}$  (Figure 5) suggests that there is a faster transition kinetics from brookite to baddeleyite than to  $\text{TiO}_2\text{-II}$  and rutile.

Upon further compression above 20 GPa up to the maximum  $P$  of 60 GPa,  $\text{TiO}_2\text{-OI}$  phase has a lower enthalpy than baddeleyite (Figure 7). Thus, the previously formed baddeleyite should transform to the  $\text{TiO}_2\text{-OI}$  phase. However, experimentally, this transition was not observed until  $P$  above  $\sim 30 \text{ GPa}$  (Figure 5a,b) or  $\sim 50 \text{ GPa}$  (Figure 5c). Such a hysteresis is related to the shear modulus of the pressure medium.<sup>60</sup> The onset transition pressure deviates more from the equilibrium value in a pressure medium with a lower shear modulus ( $G$ ).<sup>60</sup> According to ref 61, under compression, the shear modulus of helium has a magnitude that is almost the same as that of the pressure itself (e.g., at  $P = 30$  and 50 GPa,  $G \approx 30$  and 50 GPa). Using the bulk modulus data of methanol measured by Zaug et al.,<sup>62</sup> we estimated that the shear modulus of methanol is  $G \approx 14$  and 22 GPa at  $P = 30$  and 50 GPa, respectively (see the SI). If the elastic behaviors of helium and neon are similar and those of methanol and ethanol are similar, then we would expect the onset pressure of the baddeleyite  $\rightarrow \text{TiO}_2\text{-OI}$  transition in the helium/neon medium to be lower than that in the methanol–ethanol mixture. This deduction is consistent with the experimental results shown in Figure 5.

It is also possible that the non-hydrostaticity of a pressure medium (after its solidification) may contribute to the hysteresis in the baddeleyite  $\rightarrow \text{TiO}_2\text{-OI}$  transition. Results from our DFT calculations show that the non-hydrostaticity can indeed delay the transition, making baddeleyite more stable by  $\sim 0.1\text{--}0.2 \text{ kJ/mol}$  than at hydrostatic conditions (see Table S1). However, this effect is minor compared to the effect of shear modulus of a pressure medium (above).

Similar analyses can also be applied to the decompression process, which also shows a good agreement between the predicted phase transition sequences (Figure 7) with the experimental ones (Figure 5a,b). Experimentally, metastable

$\text{TiO}_2\text{-II}$  dominated during decompression below  $\sim 15 \text{ GPa}$  possibly because of the higher transition kinetics from baddeleyite to  $\text{TiO}_2\text{-II}$  than to rutile.

The above analyses show that the calculated relative enthalpy diagram of  $\text{TiO}_2$  is consistent with observations when additional degrees of freedom (from non-hydrostatic pressure) and their influence on kinetics are considered in conjunction.

## CONCLUSIONS

At room temperature and under compression up to  $\sim 60 \text{ GPa}$ , natural brookite undergoes a series of phase transitions at attainable kinetics, driven by a decrease in the free energy. Below  $\sim 21 \text{ GPa}$ , brookite exhibits similar transition behaviors in three kinds of pressure media, helium, neon, and a methanol–ethanol mixture: brookite ( $\sim 0\text{--}12 \text{ GPa}$ )  $\rightarrow \text{TiO}_2\text{-II}$  and minor rutile ( $\sim 1\text{--}21 \text{ GPa}$ )  $\rightarrow$  baddeleyite ( $\sim 12\text{--}21 \text{ GPa}$ ). A single phase of baddeleyite exists from  $\sim 21$  to 33 GPa (in helium/neon) or from  $\sim 21$  to 50 GPa (methanol–ethanol mixture). Above  $\sim 33 \text{ GPa}$  (in helium/neon) or  $\sim 50 \text{ GPa}$  (methanol–ethanol mixture) up to  $\sim 60 \text{ GPa}$ , baddeleyite transforms to  $\text{TiO}_2\text{-OI}$ . The differences in these onset pressures of the baddeleyite  $\rightarrow \text{TiO}_2\text{-OI}$  transition arise from the differences in the shear moduli of the pressure media after solidification. The non-hydrostaticity of a pressure medium at high pressure makes the baddeleyite  $\rightarrow \text{TiO}_2\text{-OI}$  transition energetically less favorable than at hydrostatic conditions. This work provides new knowledge of the natural brookite phase transitions at very high pressures (up to  $\sim 60 \text{ GPa}$ ), offering insights into how hydrostaticity and the elastic properties of a pressure medium can affect the phase transition behavior under compression. The obtained fundamental understanding of the brookite system may be transferable to other natural mineral systems.

## ASSOCIATED CONTENT

### S Supporting Information

The Supporting Information is available free of charge on the ACS Publications website at DOI: [10.1021/acsearthspacechem.8b00213](https://doi.org/10.1021/acsearthspacechem.8b00213).

Effect of non-hydrostaticity on enthalpy, XRD pattern of thin foil brookite, lattice parameters from representative Rietveld fitting, bulk moduli of  $\text{TiO}_2$  phases, and shear modulus of methanol at high pressure (PDF)

## AUTHOR INFORMATION

### Corresponding Author

\*E-mail: [hengzhong.zhang@hpstar.ac.cn](mailto:hengzhong.zhang@hpstar.ac.cn). Tel.: +86-21-80177095.

### ORCID

Hengzhong Zhang: [0000-0003-2322-2274](https://orcid.org/0000-0003-2322-2274)

### Notes

The authors declare no competing financial interest.

## ACKNOWLEDGMENTS

The high-pressure synchrotron X-ray diffraction was conducted at the high-energy beamline station 12.2.2 of Advanced Light Source, Lawrence Berkeley National Laboratory, Berkeley, CA, USA and beamline station 13-BM-C of Advanced Photon Source, Argonne National Laboratory, Argonne, IL, USA. Part of the experimental work of this

study was conducted at GeoSoilEnviroCARS (Sector 13), Partnership for Extreme Crystallography Program (PX<sup>2</sup>), Advanced Photon Source (APS), and Argonne National Laboratory. GeoSoilEnviroCARS is supported by the National Science Foundation—Earth Sciences (Grant EAR-1128799) and Department of Energy—Geosciences (Grant DE-FG02-94ER14466). PX<sup>2</sup> Program is supported by COMPRES under NSF Cooperative Agreement EAR 11-57758. Use of the Advanced Photon Source was supported by the U.S. Department of Energy, Office of Science, Office of Basic Energy Sciences, under Contract No. DE-AC02-06CH11357. We thank Tim Teague (UCB) for providing the natural brookite mineral sample and Yanping Yang (HPSTAR) for assistance in SEM sample characterization.

## ■ REFERENCES

- (1) Hwang, S. L.; Shen, P.; Chu, H. T. Nanometer-size  $\alpha$ -PbO<sub>2</sub>-type TiO<sub>2</sub> in garnet: a thermobarometer for ultrahigh-pressure metamorphism. *Science* **2000**, *288*, 321–324.
- (2) Dewhurst, J. K.; Lowther, J. E. High-pressure structural phases of titanium dioxide. *Phys. Rev. B: Condens. Matter Mater. Phys.* **1996**, *54*, R3673.
- (3) Smith, S. J.; Stevens, R.; Liu, S.; Li, G.; Navrotsky, A.; Boero-Goates, J.; Woodfield, B. F. Heat capacities and thermodynamic functions of TiO<sub>2</sub> anatase and rutile: analysis of phase stability. *Am. Mineral.* **2009**, *94*, 236–243.
- (4) Zhang, H.; Banfield, J. F. Structural characteristics and mechanical and thermodynamic properties of nanocrystalline TiO<sub>2</sub>. *Chem. Rev.* **2014**, *114*, 9613–9644.
- (5) Zhang, H.; Banfield, J. F. Understanding polymorphic phase transformation behavior during growth of nanocrystalline aggregates: insights from TiO<sub>2</sub>. *J. Phys. Chem. B* **2000**, *104*, 3481–3487.
- (6) Zhu, K. R.; Zhang, M. S.; Hong, J. M.; Yin, Z. Size effect on phase transition sequence of TiO<sub>2</sub> nanocrystal. *Mater. Sci. Eng.: A* **2005**, *403*, 87–93.
- (7) Gribb, A. A.; Banfield, J. F. Particle size effects on transformation kinetics and phase stability in nanocrystalline TiO<sub>2</sub>. *Am. Mineral.* **1997**, *82*, 717–728.
- (8) Howard, J. M. The geology of Arkansas: the natural state. *Rocks Miner.* **1989**, *64*, 270–276.
- (9) Howard, J. M. Brookite, rutile paramorphs after brookite, and rutile twins from Magnet Cove, Arkansas. *Rocks Miner.* **1999**, *74*, 92–102.
- (10) Howard, J. M.; Owens, D. R. Minerals of the Wilson springs vanadium mines: potash sulphur springs, Arkansas. *Rocks Miner.* **1995**, *70*, 154–170.
- (11) Dachille, F.; Simons, P.; Roy, R. Pressure-temperature studies of anatase, brookite, rutile and TiO<sub>2</sub>-II. *Am. Mineral.* **1968**, *53*, 1929–1939.
- (12) Yanqing, Z.; Erwei, S.; Suxian, C.; Wenjun, L.; Xingfang, H. Hydrothermal preparation and characterization of brookite-type TiO<sub>2</sub> nanocrystallites. *J. Mater. Sci. Lett.* **2000**, *19*, 1445–1448.
- (13) Buonsanti, R.; Grillo, V.; Carlino, E.; Giannini, C.; Kipp, T.; Cingolani, R.; Cozzoli, P. D. Nonhydrolytic synthesis of high-quality anisotropically shaped brookite TiO<sub>2</sub> nanocrystals. *J. Am. Chem. Soc.* **2008**, *130*, 11223–11233.
- (14) Lin, H.; Li, L.; Zhao, M.; Huang, X.; Chen, X.; Li, G.; Yu, R. Synthesis of high-quality brookite TiO<sub>2</sub> single-crystalline nanosheets with specific facets exposed: tuning catalysts from inert to highly reactive. *J. Am. Chem. Soc.* **2012**, *134*, 8328–8331.
- (15) Xu, Y.; Lin, H.; Li, L.; Huang, X.; Li, G. Precursor-directed synthesis of well-faceted brookite TiO<sub>2</sub> single crystals for efficient photocatalytic performances. *J. Mater. Chem. A* **2015**, *3*, 22361–22368.
- (16) Jamieson, J. C.; Olinger, B. High-pressure polymorphism of titanium dioxide. *Science* **1968**, *161*, 893–895.
- (17) Sato, H.; Endo, S.; Sugiyama, M.; Kikegawa, T.; Shimomura, O.; Kusaba, K. Baddeleyite-type high-pressure phase of TiO<sub>2</sub>. *Science* **1991**, *251*, 786–788.
- (18) Dubrovinskaia, N. A.; Dubrovinsky, L. S.; Ahuja, R.; Prokopenko, V. B.; Dmitriev, V.; Weber, H. P.; Osorio-Guillen, J.; Johansson, B. Experimental and theoretical identification of a new high-pressure TiO<sub>2</sub> polymorph. *Phys. Rev. Lett.* **2001**, *87*, 275501.
- (19) Dubrovinsky, L. S.; Dubrovinskaia, N. A.; Swamy, V.; Muscat, J.; Harrison, N. M.; Ahuja, R.; Holm, B.; Johansson, B. Materials science: The hardest known oxide. *Nature* **2001**, *410*, 653.
- (20) Luo, W.; Yang, S.; Wang, Z.; Wang, Y.; Ahuja, R.; Johansson, B.; Liu, J.; Zou, G. T. Structural phase transitions in brookite-type TiO<sub>2</sub> under high pressure. *Solid State Commun.* **2005**, *133*, 49–53.
- (21) Clark, S. M.; MacDowell, A. A.; Knight, J.; Kalkan, B.; Yan, J.; Chen, B.; Williams, Q. Beamline 12.2.2: an extreme conditions beamline at the Advanced Light Source. *Synchrotron Radiation News* **2012**, *25*, 10–11.
- (22) Kunz, M.; MacDowell, A. A.; Caldwell, W. A.; Cambie, D.; Celestre, R. S.; Domning, E. E.; Duarte, R. M.; Gleason, A. E.; Glossinger, J. M.; Kelez, N.; et al. A beamline for high-pressure studies at the Advanced Light Source with a superconducting bending magnet as the source. *J. Synchrotron Radiat.* **2005**, *12*, 650–658.
- (23) Prescher, C.; Prakapenka, V. B. DIOPTAS: a program for reduction of two-dimensional X-ray diffraction data and data exploration. *High Pressure Res.* **2015**, *35*, 223–230.
- (24) Toby, B. H. EXPGUI: a graphical user interface for GSAS. *J. Appl. Crystallogr.* **2001**, *34*, 210–213.
- (25) Stutzman, P. E.; Struble, L. *Instructions in Using GSAS Rietveld Software for Quantitative X-Ray Diffraction Analysis of Portland Clinker and Cement*, Technical Note NIST TN 1884; National Institute of Standards and Technology, 2015; DOI: [10.6028/NIST.TN.1884](https://doi.org/10.6028/NIST.TN.1884).
- (26) Giannozzi, P.; Andreussi, O.; Brumme, T.; Bunau, O.; Buongiorno Nardelli, M.; Calandra, M.; Car, R.; Cavazzoni, C.; Ceresoli, D.; Cococcioni, M.; et al. Advanced capabilities for materials modelling with Quantum ESPRESSO. *J. Phys.: Condens. Matter* **2017**, *29*, 465901.
- (27) Nishihara, S. *Burai 1.3, A GUI of Quantum ESPRESSO*; 2016; <http://nisihara.wixsite.com/burai>.
- (28) Blöchl, P. E. Projector augmented-wave method. *Phys. Rev. B: Condens. Matter Mater. Phys.* **1994**, *50*, 17953.
- (29) Perdew, J. P.; Burke, K.; Ernzerhof, M. Generalized gradient approximation made simple. *Phys. Rev. Lett.* **1996**, *77*, 3865.
- (30) Anisimov, V. I.; Zaanen, J.; Andersen, O. K. Band theory and Mott insulators: Hubbard U instead of Stoner I. *Phys. Rev. B: Condens. Matter Mater. Phys.* **1991**, *44*, 943.
- (31) Arroyo-de Dompablo, M. E.; Morales-García, A.; Taravillo, M. DFT + U calculations of crystal lattice, electronic structure, and phase stability under pressure of TiO<sub>2</sub> polymorphs. *J. Chem. Phys.* **2011**, *135*, 054503.
- (32) Hellenbrandt, M. The inorganic crystal structure database (ICSD)—present and future. *Crystallogr. Rev.* **2004**, *10*, 17–22.
- (33) Pauling, L.; Sturdivant, J. H. XV. The crystal structure of brookite. *Z. Kristallogr. - Cryst. Mater.* **1928**, *68*, 239–256.
- (34) Klotz, S.; Chervin, J.; Munsch, P.; Le Marchand, G. Hydrostatic limits of 11 pressure transmitting media. *J. Phys. D: Appl. Phys.* **2009**, *42*, 075413.
- (35) Gražulis, S.; Daškevič, A.; Merkys, A.; Chateigner, D.; Lutterotti, L.; Quiros, M.; Serebryanaya, N. R.; Moeck, P.; Downs, R. T.; Le Bail, A. Crystallography Open Database (COD): an open-access collection of crystal structures and platform for world-wide collaboration. *Nucleic Acids Res.* **2012**, *40*, D420–D427.
- (36) Desgreniers, S.; Lagarec, K. High-density ZrO<sub>2</sub> and HfO<sub>2</sub>: crystalline structures and equations of state. *Phys. Rev. B: Condens. Matter Mater. Phys.* **1999**, *59*, 8467.
- (37) Adams, D. M.; Leonard, S.; Russell, D. R.; Cernik, R. J. X-ray diffraction study of hafnia under high pressure using synchrotron radiation. *J. Phys. Chem. Solids* **1991**, *52*, 1181–1186.

- (38) Leger, J. M.; Tomaszewski, P.; Atouf, A.; Pereira, A. S. Pressure-induced structural phase transitions in zirconia under high pressure. *Phys. Rev. B: Condens. Matter Mater. Phys.* **1993**, *47*, 14075.
- (39) Leger, J. M.; Atouf, A.; Tomaszewski, P.; Pereira, A. S. Pressure-induced phase transitions and volume changes in  $\text{HfO}_2$  up to 50 GPa. *Phys. Rev. B: Condens. Matter Mater. Phys.* **1993**, *48*, 93.
- (40) Tompsett, G.; Bowmaker, G.; Cooney, R.; Metson, J.; Rodgers, K.; Seakins, J. M. The Raman spectrum of brookite,  $\text{TiO}_2$  ( $\text{Pbca}$ ,  $Z=8$ ). *J. Raman Spectrosc.* **1995**, *26*, 57–62.
- (41) Iliev, M. N.; Hadjiev, V. G.; Litvinchuk, A. P. Raman and infrared spectra of brookite ( $\text{TiO}_2$ ): experiment and theory. *Vib. Spectrosc.* **2013**, *64*, 148–152.
- (42) Li, Q.; Liu, R.; Liu, B.; Wang, L.; Wang, K.; Li, D.; Zou, B.; Cui, T.; Liu, J.; Chen, Z.; Yang, K. Stability and phase transition of nanoporous rutile  $\text{TiO}_2$  under high pressure. *RSC Adv.* **2012**, *2*, 9052–9057.
- (43) Li, Q. J.; Liu, B. B. High pressure structural phase transitions of  $\text{TiO}_2$  nanomaterials. *Chin. Phys. B* **2016**, *25*, 076107.
- (44) Li, Q.; Liu, R.; Cheng, B.; Wang, L.; Yao, M.; Li, D.; Zou, B.; Cui, T.; Liu, B. B. High pressure behaviors of nanoporous anatase  $\text{TiO}_2$ . *Mater. Res. Bull.* **2012**, *47*, 1396–1399.
- (45) Huberty, J.; Xu, H. Kinetics study on phase transformation from titania polymorph brookite to rutile. *J. Solid State Chem.* **2008**, *181*, 508–514.
- (46) Huang, Y.; Chen, F.; Li, X.; Yuan, Y.; Dong, H.; Samanta, S.; Yu, Z.; Rahman, S.; Zhang, J.; Yang, K.; Yan, S.; Wang, L. Pressure-induced phase transitions of exposed curved surface nano- $\text{TiO}_2$  with high photocatalytic activity. *J. Appl. Phys.* **2016**, *119*, 215903.
- (47) Dylla, A. G.; Henkelman, G.; Stevenson, K. J. Lithium insertion in nanostructured  $\text{TiO}_2$ (B) architectures. *Acc. Chem. Res.* **2013**, *46*, 1104–1112.
- (48) Haines, J.; Leger, J.; Schulte, O. The high-pressure phase transition sequence from the rutile-type through to the cotunnite-type structure in. *J. Phys.: Condens. Matter* **1996**, *8*, 1631.
- (49) Lowther, J.; Dewhurst, J.; Leger, J.; Haines, J. Relative stability of  $\text{ZrO}_2$  and  $\text{HfO}_2$  structural phases. *Phys. Rev. B: Condens. Matter Mater. Phys.* **1999**, *60*, 14485.
- (50) Mei, Z. G.; Wang, Y.; Shang, S.; Liu, Z. K. First-principles study of the mechanical properties and phase stability of  $\text{TiO}_2$ . *Comput. Mater. Sci.* **2014**, *83*, 114–119.
- (51) Nishio-Hamane, D.; Shimizu, A.; Nakahira, R.; Niwa, K.; Sano-Furukawa, A.; Okada, T.; Yagi, T.; Kikegawa, T. The stability and equation of state for the cotunnite phase of  $\text{TiO}_2$  up to 70 GPa. *Phys. Chem. Miner.* **2010**, *37*, 129–136.
- (52) Mei, Z. G.; Wang, Y.; Shang, S. L.; Liu, Z. K. First-principles study of lattice dynamics and thermodynamics of  $\text{TiO}_2$  polymorphs. *Inorg. Chem.* **2011**, *50*, 6996–7003.
- (53) Fu, Z.; Liang, Y.; Wang, S.; Zhong, Z. Structural phase transition and mechanical properties of  $\text{TiO}_2$  under high pressure. *Phys. Status Solidi B* **2013**, *250*, 2206–2214.
- (54) Swamy, V.; Wilson, N. C. First-principles calculations of the pressure stability and elasticity of dense  $\text{TiO}_2$  phases using the B3LYP hybrid functional. *J. Phys. Chem. C* **2014**, *118*, 8617–8625.
- (55) Liu, Q. J.; Ran, Z.; Liu, F. S.; Liu, Z. T. Phase transitions and mechanical stability of  $\text{TiO}_2$  polymorphs under high pressure. *J. Alloys Compd.* **2015**, *631*, 192–201.
- (56) Trail, J.; Monserrat, B.; Lopez Ríos, P. L.; Maezono, R.; Needs, R. J. Quantum Monte Carlo study of the energetics of the rutile, anatase, brookite, and columbite  $\text{TiO}_2$  polymorphs. *Phys. Rev. B: Condens. Matter Mater. Phys.* **2017**, *95*, 121108.
- (57) Wu, X.; Holbig, E.; Steinle-Neumann, G. Structural stability of  $\text{TiO}_2$  at high pressure in density-functional theory based calculations. *J. Phys.: Condens. Matter* **2010**, *22*, 295501.
- (58) Che, X.; Li, L.; Zheng, J.; Li, G.; Shi, Q. Heat capacity and thermodynamic functions of brookite  $\text{TiO}_2$ . *J. Chem. Thermodyn.* **2016**, *93*, 45–51.
- (59) Banfield, J. F.; Veblen, D. R. Conversion of perovskite to anatase and  $\text{TiO}_2$ (B): a TEM study and the use of fundamental building blocks for understanding relationships among the  $\text{TiO}_2$  minerals. *Am. Mineral.* **1992**, *77*, 545–557.
- (60) Barge, N. V.; Boehler, R. Effect of non-hydrostaticity on the  $\alpha$ - $\epsilon$  transition of iron. *High Pressure Res.* **1990**, *6*, 133–140.
- (61) Grechnev, A.; Tretyak, S. M.; Freiman, Y. A.; Goncharov, A. F.; Gregoryanz, E. Elastic anisotropy and poisson's ratio of solid helium under pressure. *Phys. Rev. B: Condens. Matter Mater. Phys.* **2015**, *92*, 024102.
- (62) Zaug, J. M.; Slutsky, L. J.; Brown, J. M. Equilibrium properties and structural relaxation in methanol to 30.4 GPa. *J. Phys. Chem.* **1994**, *98*, 6008–6016.